Chemical Engineering Journal 399 (2020) 125670

Contents lists available at ScienceDirect

Chemical Engineering Journal

journal homepage: www.elsevier.com/locate/cej

Polyhedral TiO_2 particle-based cathode for Li-S batteries with high volumetric capacity and high performance in lean electrolyte

Jaehyun Lee, Jun Hyuk Moon*

Department of Chemical and Biomolecular Engineering, Sogang University, 35 Baekbeom-ro, Mapo-gu, Seoul 04107, Republic of Korea

HIGHLIGHTS

- Formation of polyhedral TiO_2 particles by physical method.
- High tap-density electrodes by assembly of polyhedral TiO_2 particles.
- Achievement of high volumetric capacity of 1145 mAh/cm^3.
- Excellent capacity retention even in lean electrolyte.

ARTICLE INFO

Keywords:
Polyhedral structure
Tap density
Lean electrolyte
Titanium dioxide
Lithium sulfur batteries

ABSTRACT

Achieving high volumetric capacity in Li-S batteries featuring light weight opens up unique applications. To address this, we demonstrate a high tap-density cathode based on polyhedral TiO_2 (poly-TiO_2) particles. The poly-TiO_2 particles are obtained by fracturing 3D ordered macroporous TiO_2 structure. Poly-TiO_2 particles achieve high packing densities by assembly of surface-to-surface contact. Compared to commercial TiO_2 nanoparticles, poly-TiO_2 exhibits an apparent tap-density of about 6 times higher. We prepare a Li-S battery with a poly-TiO_2 particle-assembled film as the host of the sulfur. The poly-TiO_2 particle cell exhibits a volumetric capacity of 1145 mAh/cm^3, which is about 9 times higher than the TiO_2 nanoparticle cathode cell. The poly-TiO_2 cathode with high tap-density shows excellent performance in lean electrolyte condition. Under extremely lean electrolyte conditions with an E/S value of 2.8, the poly-TiO_2 cell exhibits a high capacity of 607 mAh/g at 1C-rate.

1. Introduction

Lithium-sulfur (Li-S) batteries are attracting attention not only because of their high energy density but also because of their unique advantages in light weight [1–3]. As a host of sulfur having low electrical conductivity (5×10^{-30} S/cm at 25 °C) and having a high solubility intermediate (Li polysulfide (Li PS)) in electrolyte, various porous carbon hosts (e.g., micro- or mesoporous carbon, carbon nanotubes, and graphene) have been widely applied [4–12]. Recently, much effort has been devoted to the inclusion of various metal compounds with high chemical affinity for PS ions [13–20].

In most studies, the energy storage of Li-S batteries has been evaluated based on its gravimetric capacity, i.e., the capacity based on the mass of sulfur or the mass of the cathode electrode, but considering the inherent lightweight characteristics (due to the low density of sulfur) of Li-S batteries, a rather important performance metric is volumetric capacity [21–24]. Compact Li-S batteries can find unique applications such as drones or unmanned aerial vehicles where both light weight and compact size are important [25,26]. As a few studies to address this, Wang and co-workers used a compact layer host of rGO-VS_2 sheets to obtain high tap-density electrodes and achieve high volumetric capacity of 1182.1 mAh/cm^3 at 1C [25]. Chen and co-workers exploited the assembly of porous carbon spheres in a polymodal size distribution to achieve high tap-density electrodes and thereby a high volumetric capacity of 495 mAh/cm^3 [27]. Most of these studies have controlled the assembly of carbon materials to achieve high tap-density electrodes and high volumetric capacity. However, considering the use of high content metal compounds in recent studies, the design of these particles to obtain high tap-density electrodes is rather demanding.

In this study, we introduce a polyhedral TiO_2 (poly-TiO_2) particle-based host to achieve a high volumetric capacity. Previously, TiO_2 nanotubes [28], hierarchical sphere [29], mesoporous TiO_2 [30] and TiO_2 nanofibers [31] have been applied; however they were for effective adsorption by TiO_2 with high surface area (see Table S1). In

* Corresponding author.
E-mail address: junhyuk@sogang.ac.kr (J.H. Moon).

https://doi.org/10.1016/j.cej.2020.125670
Received 24 January 2020; Received in revised form 25 May 2020; Accepted 26 May 2020
Available online 30 May 2020
1385-8947/

addition, carbon materials coated with nanoparticles or porous shells of TiO_2 have been applied; in this case as well, the coating of TiO2 was for high adsorption of LiPS [32,33]. Unlike these studies, the poly-TiO2 is intended to form high tap-density electrodes [34–36]. We compare poly-TiO_2 with commercially available nanocrystalline TiO_2 (nc-TiO_2) spherical particles. The poly-TiO_2 particles achieve an apparent tap-density that is up to 6 times higher than that of the nc-TiO_2 particles. This results in a remarkably high volumetric capacity of 1145 mAh/cm^3 for the poly-TiO_2-based cathode, which is 9 times higher than that of the nc-TiO_2-particle-based cathode. In addition, poly-TiO_2 cathode cell exhibits excellent performance under "lean electrolyte" conditions due to its high tap density. Even when the ratio of the electrolyte volume/sulfur mass (the E/S ratio) is reduced to about 1/4, the poly-TiO_2 exhibits an excellent capacity retention of 84%.

2. Experimental

2.1. Preparation of the poly-TiO_2 particles

Monodispersed polystyrene particles were synthesized by dispersion polymerization using polyvinylpyrrolidone (MW = 49,000, Junsei) as a stabilizer. Briefly, we used a thermal initiator, 2,2-azobis(2-methylbutyronitrile) (1 wt% of styrene, Aldrich), a stabilizer, poly(N-vinylpyrrolidone) (1 wt% in solution) and ethanol (Aldrich) as the solvent. The polymerization proceeded for 16 h at 80C. The polystyrene particles were dispersed in ethanol and dried at 60 ˚C for 12 h, and this colloidal crystal was applied as a template. When the colloidal solution containing TiO_2 nanoparticles (average size 15 nm, Nanoamor Inc.) was dropped onto the template, it was infiltrated by capillary action into the pores between the particles. Then, 3D, ordered, macroporous TiO_2 was obtained by removing the template through sintering at 500 ˚C. We weakly ground the 3D TiO_2 powder with a mortar, dispersed it in water and applied ultrasonic waves to obtain poly-TiO_2 particles. The frequencies of the ultrasonic waves were 20 KHz and 80 W. After that, weak centrifugal separation was repeated at 4000 rpm to remove any fine particles, and poly-TiO_2 of comparatively uniform size was obtained.

2.2. Li-S cell preparation and characterization

The poly-TiO_2 assembly was loaded with sulfur by melt diffusion; Sulfur powder and poly-TiO_2 particles mixed at a ratio of 6.5:3.5 were placed in an autoclave reactor and maintained at 155 ˚C for 12 hrs. Then, a slurry was prepared by mixing the sulfur-loaded poly-TiO_2, a single-walled carbon nanotube (Merck)/carbon nanoparticle (Super-P, Alfa Aesar) conductive agent and a polyacrylonitrile-based binder. Typically, poly-TiO_2 particles, the conducting agent, and the binder were mixed at 7: 2: 1. However, this ratio was adjusted to 6: 2: 2 for the preparation of high sulfur loading electrodes. The slurry was cast on an aluminum foil current collector by the doctor blade method. The mixing ratio of active material, conducting agent and binder was 7:2:1. The film was dried at 60 ˚C for 12 h and punched into disk electrodes. We fabricated a CR2032 coin-type cell by assembling this electrode with Li metal foil (1 mm thickness) and a polypropylene membrane. The cell was prepared under dry conditions with a humidity less than 0.3%. The battery performance was evaluated using a Maccor 4300 test system. The electrolyte was prepared by mixing 1 M bis(trifluoromethane)sulfonylimide lithium (LiTFSI) with 0.2 M $LiNO_3$ as the additive in a 1:1 mixture of 1,3-dioxolane (DOX)/dimethylethane (DME). The cell was assembled under dry conditions with less than 0.3% humidity. The CV curves were obtained at a scan rate of 0.01 mV s^{-1} with applied voltages between 1.7 and 2.8 V vs. $Li/Li^{\pm}$. The galvanostatic charge/discharge cycles were obtained over the voltage range of 1.7–2.8 V at various C values (0.1–2.0C). The electrochemical impedance spectra were obtained at a constant perturbation amplitude of 10 mV in the frequency range between 1 MHz and 0.1 Hz.

2.3. Materials characterization

For the measurement of adsorption to Li_2S_4 or Li_2S_6, we dissolved Li_2S or sulfur in 5 mM/L in 1:1 (v/v) DOL/DME and dispersed TiO_2 particles at a concentration of 10 mg/L. Adsorption concentrations of Li PS were quantified using UV–Vis absorbance. Specifically, a decrease in the decrease of the peak at a wavelength of 290 nm was observed (see Fig. S12.) The surface morphologies were observed using field-emission SEM (FESEM, JSM-7800F JEOL). TEM images were obtained using a transmission electron microscope (JEM-4300, JEOL). The crystal structure was analyzed by XRD (Rigaku). X-ray photoelectron spectroscopy (XPS) was measured using a Leybold spectrometer with an Al Ka monochromatic beam (1486.6 eV) with an input power of 150 W (ESCALAB250 XPS system, Theta Probe System). The concentration of lithium polysulfide ions was analyzed by UV–Vis spectrophotometry (UV-2550, Shimadzu). TGA was performed by heating the samples to an appropriate temperature at a heating rate of 10 ˚C/min (TGA-50H, SHIMADZU). The specific surface areas were obtained using the Barrett–Emmett–Teller (BET) method with a porosimeter (ASAP 2020, Micrometrics Inc.).

3. Results and discussion

To produce poly-TiO_2 particles, we utilized a physical method to break up ordered macroporous TiO_2. We first fabricated 3D ordered macroporous TiO_2 by applying a colloidal crystal of a polymer sphere as a template, infiltrating the TiO_2 precursor, and then selectively removing polymer particles through heat treatment (see the polymer colloidal crystal in Fig. S1). We applied ultrasound to break up the ordered, macroporous TiO_2; the TiO_2 precursor is difficult to penetrate in the vicinity of the spherical particles in contact with the precursor, resulting in the formation of thin, mechanically weak TiO_2, which is easily crushed. As a result, a particle centered around TiO_2 penetrating the cavity between particles is obtained. This particle has a polyhedral morphology with concave surfaces, and the surfaces of the various particles around the cavity are reversed. These concave surfaces ensure sufficient space for contact with the electrolyte even when assemble with high tap-density.

SEM images of 3D ordered macroporous TiO_2 and poly-TiO_2 particles are shown in Fig. S2. We dispersed crushed particles in solution and centrifuged them to select poly-TiO_2 particles with relatively uniform size. The poly-TiO_2 particles had sizes ranging from 1 μm to 1.3 μm. We measured the specific volume of the poly-TiO_2 particles and compare it to that of commercially available nc-TiO_2 nanoparticles. For samples with the same mass, the poly-TiO_2 particles occupy a volume almost 6 times smaller than the commercially available nc-TiO_2 nanoparticles (see Fig. S3). The apparent tap-density of the poly-TiO_2 particles and nc-TiO_2 particles was 0.6 g/cm^3 and 0.1 g/cm^3, respectively. In Fig. 1a and 1b, we compare the SEM images of the assemblies obtained by slowly drying poly-TiO_2 and nc-TiO_2 particles dispersion. The poly-TiO_2 image shows a tightly packed morphology, while the nc-TiO_2 image shows sparse packing of secondary aggregated particles several micrometers in size. Fig. 1c shown the high-magnification TEM images of poly-TiO_2. Poly-TiO_2 is composed of TiO_2 nanoparticles in the 12–22 nm size range, nc-TiO_2 is composed of nanoparticles in the 30–50 nm size range. (see Fig. S4) The poly-TiO_2 has a higher specific area due to the smaller size of the particles that make up it. Fig. 1d displays the BET isotherm of the poly-TiO_2 particles; the BET surface area was approximately 100 m^2/g, which is about 3 times larger than the surface area of nc-TiO_2 particles was approximately 35 m^2/g (see Fig. S5). The poly-TiO_2 has a higher specific area due to the smaller size of the particles that make up it. The XRD pattern of the poly-TiO_2 particles is shown in Fig. S6. The peaks observed at 25.4˚, 37.9˚, 48.1˚, 54.2˚ and 55.2˚ correspond to the (1 0 1), (0 0 4), (2 0 0), (1 0 5) and (2 1 1) planes, respectively, of anatase TiO_2 [37].

We measured the contact angle of a molten sulfur drop on each film

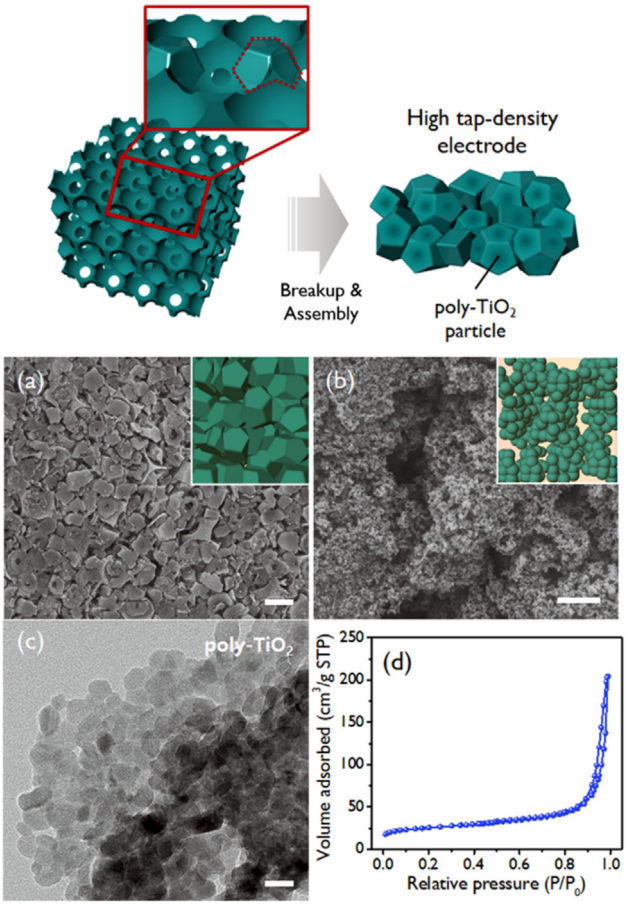

Fig. 1. Schematic illustration of the synthesis of poly-TiO_2 particles for their application in a cathode for Li-S batteries. Characterizations of poly-TiO_2 particles. SEM images of the assembly film of (a) poly-TiO_2 and (b) nc-TiO_2 particles. The scale bar of Fig. (a) – (b) is 1 μm. (c) TEM image of secondary particles of poly-TiO_2. The scale bar is 20 nm (d) N_2 adsorption–desorption isotherms of poly-TiO_2.

with poly-TiO_2 and nc-TiO_2 assembled. The poly-TiO_2 film showed a remarkably low contact angle of 11° and immediate penetration of the film by sulfur while the nc-TiO_2 film showed partial wetting and slow sulfur absorption into the film, as observed in Fig. S7. The high affinity of poly-TiO_2 for sulfur may be attributed to its assembled structure. The poly-TiO_2 film has a denser structure with finer pores between particles than the nc-TiO_2 film, which induces stronger capillary action [38].

We evaluated the chemical adsorption of Li PS anions on poly-TiO_2 particles. Among various metal oxides, TiO_2 shows a relatively high affinity for Li PS; the hydrophilic Ti-O groups and hydroxyl groups on the TiO_2 surface have an ability to adsorb Li PS anions [19,38,39]. Fig. 2a shows the decrease in the solution concentration of PS anions over time in solutions containing poly-TiO_2 and nc-TiO_2 particles. The poly-TiO_2 particles show 2 times faster adsorption than the nc-TiO_2 particles. This fast adsorption may be due to the large specific surface area of poly-TiO_2. Fig. 2b compares the digital camera images of these solutions after 12 h (see also Fig. S8); the solution containing poly-TiO_2 is clearer due to the adsorption of PS in solution. The XPS spectrum of poly-TiO_2 after adsorption of Li PS is observed in Fig. 2c (The XPS spectrum for nc-TiO_2 is shown in Fig. S9). This shows peaks at approximately 163 eV and 164.2 eV as observed in Fig. 2c, which correspond to "terminal" and "bridging" sulfur (S_T and S_B), respectively, confirming the adsorption of long-chain Li_2S_6 [40,41]. The spectrum also shows the intense shoulder at 166–171 eV, which indicates a thiosulfate group. We also identify a peak at approximately 168 eV, which corresponds to a polythionate group. The presence of these functional groups indicate the catalytic conversion of the adsorbed PS anion, that is, the reduction of Li_2S_6 to $S_2O_3^{2-}$ [42,43]. It has been reported that TiO_2 is capable of reducing adsorbed anions with a more positive redox potential than PS anions [38,43].

We fabricated a Li-S battery cell by assembling a composite cathode of sulfur/poly-TiO_2 particle cathode, a Li-foil anode and a polypropylene membrane separator, where the cathode contains a single-walled carbon nanotube as a conducting agent and a polyacrylonitrile-based binder, as described in Fig. 3a. The weight of sulfur and poly-TiO_2 composite was 80% of the total electrode weight, and the S content was approximately 65% of the total active material (see Fig. S10). We also prepared a Li-S cell containing a nc-TiO_2-based cathode for comparison. Fig. S11 displays the cross-sectional SEM images of the sulfur-loaded, poly-TiO_2 and nc-TiO_2 based electrodes; here, the poly-TiO_2 electrode exhibits a more compact film than the nc-TiO_2 electrode. Additionally, it is observed that sulfur is more uniformly distributed in the poly-TiO_2 assembled electrode than the nc-TiO_2 electrode. Fig. 3b shows the SEM image of the sulfur-impregnated poly-TiO_2 film and the elemental maps of Ti and S. Sulfur, in the form of particles of approximately 10–100 nm, can be seen to be uniformly mixed with TiO_2, but a large bulk sulfur residue can be observed in the nc-TiO_2 film (Fig. S12).

We display the cyclic voltammetry curves of poly-TiO_2cathode cell for various discharge cycles (1st − 4th) and various scan rates (0.1C to 2C) in the 1.7–2.8 (vs. Li/Li^{+}) region in Fig. 3c and 3d, while the cyclic voltammetry curves of nc-TiO_2cathode cell shows in Fig. S13. The cathodic scan for both curves shows reduction peaks at 2.31 and 2.02 V, indicating the formation of long-chain PS (Li_2S_x, x = 4–8) and short-chain PS (Li_2S_x, x = 1–4). The anodic scan shows the oxidation peak at 2.35 V transformed from the short-chain PS (Li_2S, x greater than 2) to S_8 [44,45]. We observe a weak shoulder peak at approximately 1.9 V that represents anodic delithiation in anatase TiO_2 [46]. In the poly-TiO_2cathode cell, the redox peaks did not show a significant shift at various cycles and scan rates, whereas the nc-TiO_2 electrode exhibited a shift and decrease in peak intensity as the cycle number and scan rate

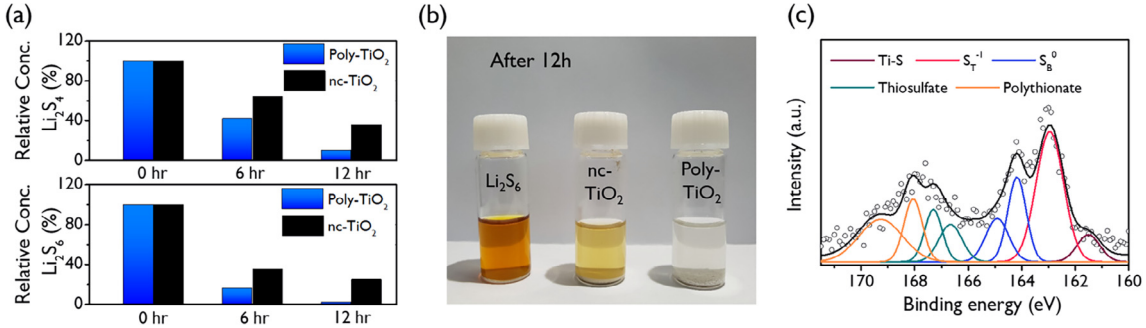

Fig. 2. (a) Concentrations of Li PS over time in Li PS solution containing poly-TiO_2 and nc-TiO_2 particles. (b) Digital image of the Li PS solution containing poly-TiO_2 or nc-TiO_2 after 12 hrs. (5 mmol/g Li_2S_6 solution containing nc-TiO_2 and poly-TiO_2) (c) High-resolution XPS of S 2p spectra of Li PS-adsorbed poly-TiO_2.

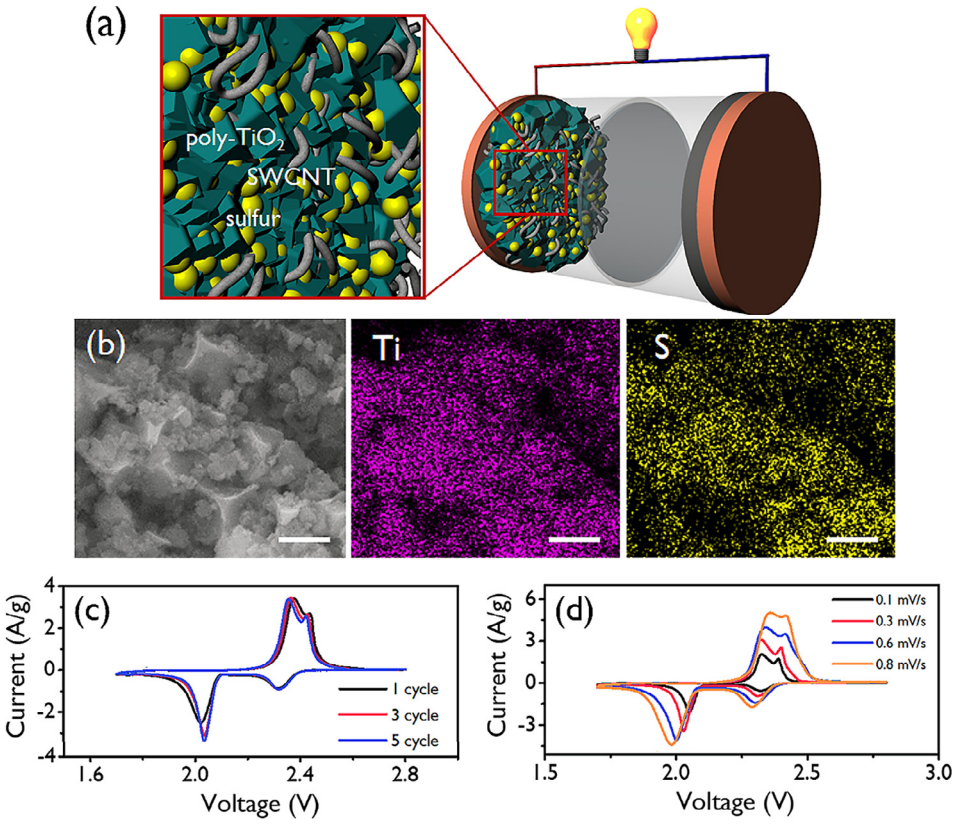

Fig. 3. (a) Schematic illustration of Li-S battery cell with poly-TiO_2-based cathode. (b) SEM image of sulfur-impregnated poly-TiO_2 and elemental mapping of Ti (pink) and S (yellow). The scale bar is 1 μm. CV curves of poly-TiO_2/S electrode Li-S cells at (c) various cycles (scan rate of 0.1 mV/s) and (d) at various scan rates. (For interpretation of the references to colour in this figure legend, the reader is referred to the web version of this article.)

increase. In addition, we observed lower onset potentials with the poly-TiO_2 particle electrodes than the nc-TiO_2 electrodes. These results show a more reversible and kinetically favorable sulfur transformation occurs on the poly-TiO_2 particles [47].

We also display the charge/discharge profiles at various C rates from 0.1C to 2C for poly-TiO_2cathode cells in Fig. 4a, while the charge/discharge profiles at various C rates for nc-TiO_2cathode cell shows in Fig. S14. The capacities at various C rates from 0.1C to 2C are also displayed in Fig. 4b; the capacities of poly-TiO_2 and nc-TiO_2 particles cells of 1st cycle at 0.1C are 1300 mAh/g and 1140 mAh/g, respectively, and show a retention of capacity of approximately 58% and 47% at 20 times increase in current density, respectively. For the poly-TiO_2

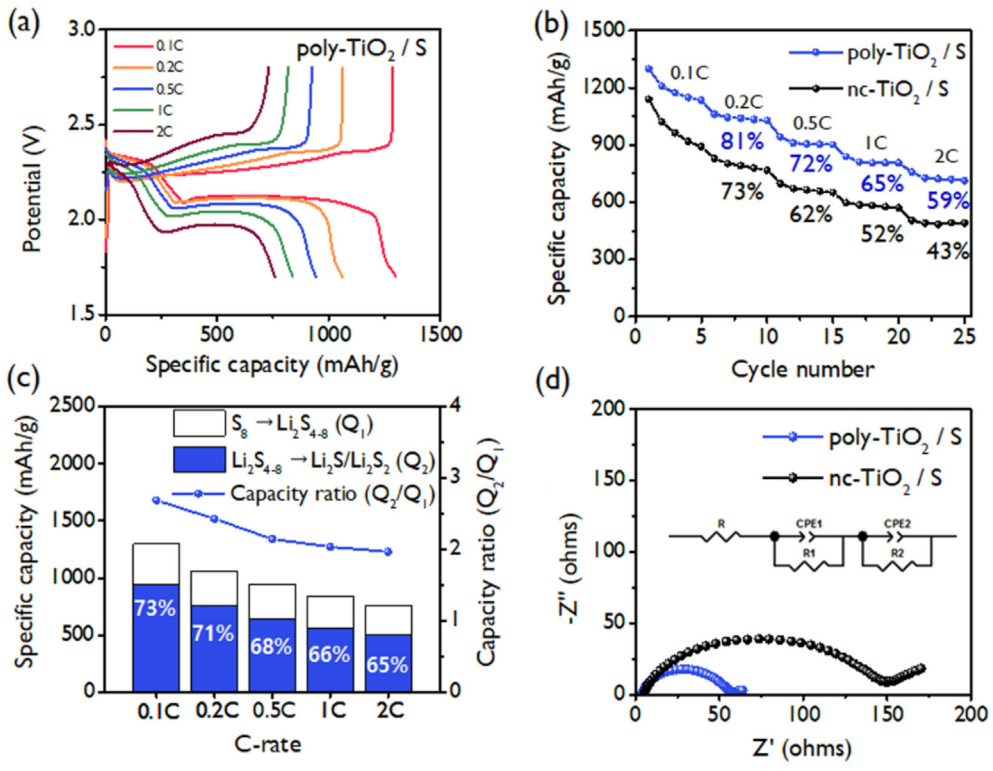

Fig. 4. (a) Charge/discharge profiles at various C rates from 0.1C to 2C for poly-TiO_2/S cells. (b) Rate performance at various C rates from 0.1C to 2C for poly-TiO_2/S. (c) Capacity contributions of high-order polysulfide conversion (Q_1) and low-order polysulfide conversion (Q_2) and the Q_2/Q_1 ratios at various C rates for the poly-TiO_2/S electrode cells. (d) Nyquist plots for poly-TiO_2/S electrodes. The inset image shows the equivalent circuit.

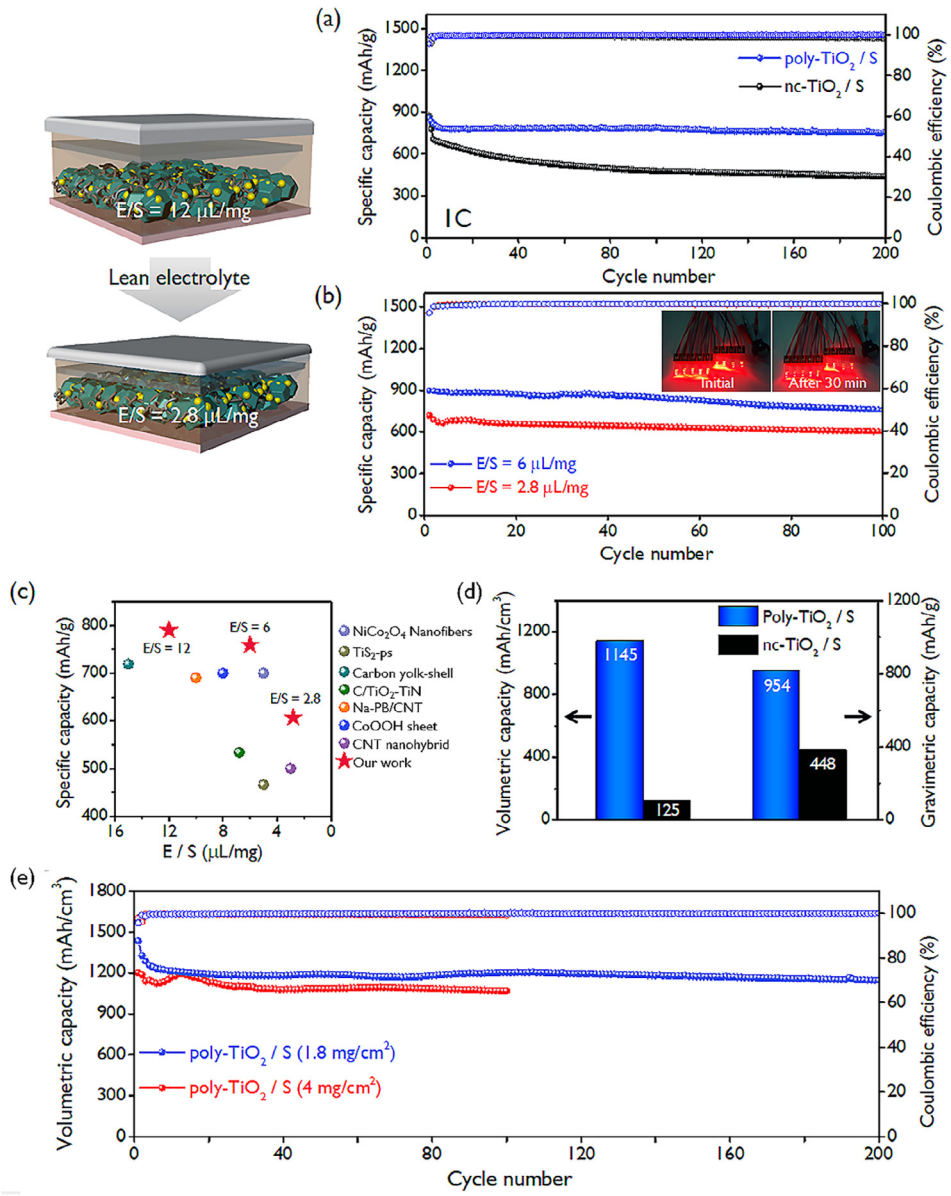

Fig. 5. (a) Cycling performance of poly-TiO_2 and nc-TiO_2 cathode cells at 1C for 200 cycles (sulfur loading = 1.2 mg/cm^2, E/S = 12 μl/mg. (volume of electrolyte solution (E), weight of sulfur (s)) (b) Cycling performance of the poly-TiO_2/S electrode (sulfur loading = 1.2 mg/cm^2) under the lean electrolyte conditions of E/S = 6 μl// mg and E / S = 2.8 μl/mg, respectively. Inset is digital images of LED lamps powered by poly-TiO_2 cells. (c) Cycling performance under lean electrolyte conditions of poly-TiO_2 compares the capacity values of recent results with an E/S ratio of less than 15. (d) Comparison of volumetric capacity and gravimetric capacity of poly-TiO_2 and nc-TiO_2 cathode cells. These capacities are capacity values at 200 cycles with 1.8 mg/cm^2 sulfur loading and 0.5C conditions. (e) The volumetric capacity of the poly-TiO_2 electrode cell according to charging/discharging cycles at 0.5C with low sulfur loading (1.8 mg/cm^2) or high sulfur loading (4.0 mg/cm^2) conditions.

and nc-TiO_2 electrodes, the capacity values extracted from the plateau at 2.1 V and 2.3 V and their ratios are compared in Fig. 4c and S12. Ideally, the capacity at the 2.1 V plateau is three times that at the 2.3 V plateau, yielding a ratio of Q_2/Q_1 of three. However, the reduction of elemental S_8 to higher order polysulfides ($S_8 \rightarrow Li_2S_8^{4-}$) is sluggish and thus incomplete; thus, the value of Q_2/Q_1 is usually less than three [48,49]. The ratios of Q_2/Q_1 for the poly-TiO_2 electrode are 2.69 at 0.1C and 1.97 at 2C; the ratios for the nc-TiO_2 electrode are 2.58 at 0.1C and 1.25 at 2C. The ratio of the poly-TiO_2 sample is higher, especially at high rates. This comparison confirms the superior kinetics of the sulfur redox reaction with the poly-TiO_2 particles. (See the further information in Fig. S15.) We analyse the resistance in the electrochemical reaction by electrochemical impedance spectroscopy. Fig. 4d compares the Nyquist plots for poly-TiO_2 and nc-TiO_2 electrodes. The plot shows a semicircle in the frequency range of 1 MHz–0.1 Hz and then a straight line in the higher frequency range; the semicircle corresponds to the charge transfer resistance (R_{ct}), and the slope of the straight line relates to the solid-state diffusion [50,51]. The R_{ct} of poly-TiO_2 electrode is about 55 O, which is 3 times smaller than the R_{ct} of the nc-TiO_2 electrode (~150 O). The poly-TiO_2 electrode shows much lower charge transfer resistance than the nc-TiO_2 electrode, confirming the rapid kinetics in the poly-TiO_2 electrode.

The cycle performance of the poly-TiO_2 and nc-TiO_2 electrode cells is displayed in Fig. 5a. The result shows the specific capacity of these cells for charge/discharge cycling at 1C. The capacity retention of poly-TiO_2 at 1C was 88% after 200 cycles, but only 36% for nc-TiO_2. The excellent capacity stability of poly-TiO_2 cell indicates a more complete utilization of sulfur, which is responsible for the fast sulfur transformation in poly-TiO_2 [22,25]. Here, we evaluate the cell performance with a low volume of electrolyte, i.e., “lean electrolyte” conditions, as shown in Fig. 5b. From a practical point of view, the use of a small amount of electrolyte is favorable for achieving high energy densities, but large reductions in both capacity and long-term stability are often observed under lean electrolyte conditions [3,18,23,52]. When the electrolyte volume relative to the sulfur mass (E/S ratio) is reduced from 12 μl/mg to 6 μl/mg and 2.8 μl/mg, the poly-TiO_2 cells for each condition achieve a capacity retention of 85% and 84%, respectively, as displayed in Fig. 5b, while the nc-TiO_2 cell shows a capacity retention of 71% and 12%, respectively (see Fig. S16). Inset image shows the driving of 9 LEDs (1.8 V, ~ 20 mA) using a poly-TiO_2 Li-S cell fabricated under lean electrolyte conditions, and the LEDs are illuminated with similar brightness for 30 min. The poly-TiO_2 electrode exhibits

excellent cell performance under lean electrolyte conditions.

Fig. 5c and Table S2 compares the capacity values after cycles of recent results with an E/S ratio of less than 15. Our poly-TiO_2 electrode achieves higher specific capacity even at lower E/S ratio. In particular, the condition of E/S = 2.8 is the lowest value, i.e., the most "lean electrolyte" condition, compared to the previous results, yet poly-TiO_2 has a high capacity value of 607 mAh/g (1C). Recently, Gan and co-workers have observed that poor cell performance at low E/S conditions is caused by the presence of high sulfur ions and corrosion of the lithium anode thereby [53]. The low porosity poly-TiO_2 electrode lowers the critical volume requirement of the electrolyte and thereby maintains cell cycle stability [54]. The poly-TiO_2 electrode with high tap-density is advantageous for obtaining a high volumetric capacity [22,25,55]. The specific capacity and volumetric capacity of poly-TiO_2 and nc-TiO_2 cells after 200 cycles is compared in Fig. 5d. Here, the volumetric capacity of poly-TiO_2 is 1145 mAh/cm^3 at a specific capacity of 954 mAh/g, a sulfur loading of 1.8 mg/cm^2, and a thickness of the electrode (see Fig. S9) of 15 μm. Note that the poly-TiO_2 cell exhibits a specific capacity about 2 times higher than that of nc-TiO_2 but a volumetric capacity more than 9 times higher than that of nc-TiO_2. Even at high loading of sulfur, the volumetric capacity of poly-TiO_2 is 9 times higher than that of nc-TiO_2. Fig. 5e shows the volumetric capacity of the poly-TiO_2 electrode cell according to charge/discharge cycle at 0.5C with low loading (1.8 mg/cm^2) or high loading (4.0 mg/cm^2) conditions. The volumetric capacity was obtained by a conventional method based on the volume of the cathode [56]. Specifically, the volumetric capacity was obtained by multiplying the specific capacity (mAh/g_{sulfur}) by the areal sulfur loading (mg_{sulfur}/cm^2) of the cathode, and dividing it by the thickness (μm) of the cathode. The capacity of the nc-TiO_2 electrode at 0.5C is also displayed in Fig. S17. Our volumetric capacity values are superior to those of previous results highlighting high tap-density cathodes. Wang and co-worker fabricated high tap-density electrodes from mesoporous carbon/carbon nanotubes and obtained a capacity per volume of 800 mAh/cm^3 for 100 cycles with 4 mg/cm^2 sulfur loading [22]. Chen and coworker fabricated compact electrodes with nitrogen-doped carbon paritcles with a polymodal particle size distribution and obtained a volumetric capacity of 495 mAh/cm^3 after 100 cycles with 5.4 mAh/cm^2 sulfur loading [27]. Compared to these, our results achieve up to 2.3 times higher values, even after longer cycles.

4. Conclusions

We demonstrated facile methods of preparing polyhedral TiO_2 particles and their assembled electrodes with high tap-density for Li-S batteries with high volumetric capacity. The polyhedral particles were obtained by "physical fracturing" of a 3D ordered macroporous structure. Compared with commercial nc-TiO_2, poly-TiO_2 showed an apparent tap-density approximately 6 times higher. The high packing density greatly improved sulfur penetration by greater capillary action and formed a uniform sulfur composite electrode. When applied as the cathode for a Li-S battery, the poly-TiO_2 electrode with a high tap-density showed stable operation even under lean electrolyte conditions. Under the condition of 2.8 μl/mg S, the poly-TiO_2 electrode exhibited a specific capacity reduction of only 84%, while the commercial TiO_2 electrode showed a large decrease of 12%. Finally, the poly-TiO_2 cathode cells achieved a very high volumetric capacity, 1145 mAh/cm^3, which is 9.1 times higher than that of nc-TiO_2. Our results present a new perspective for developing high-performance Li-S cells with metal oxide-based electrodes featuring high tap-density rather than the typical high specific area microporous structure.

Declaration of Competing Interest

The authors declare that they have no known competing financial interests or personal relationships that could have appeared to influence the work reported in this paper.

Acknowledgements

This work was supported by National Research Foundation of Korea (grant No. 2019R1A2C2009123). The Korea Basic Science Institute is also acknowledged for the SEM, TEM and XPS measurements.

Appendix A. Supplementary data

Supplementary data to this article can be found online at https://doi.org/10.1016/j.cej.2020.125670.

References

[1] P.G. Bruce, S.A. Freunberger, L.J. Hardwick, J.-M. Tarascon, Li–O2 and Li–S batteries with high energy storage, Nat. Mater. 11 (2011) 19.
[2] M. Armand, J.M. Tarascon, Building better batteries, Nature 451 (2008) 652.
[3] S.-H. Chung, C.-H. Chang, A. Manthiram, Progress on the Critical Parameters for Lithium-Sulfur Batteries to be Practically Viable, Adv. Funct. Mater. 28 (2018) 1801188.
[4] H.-J. Peng, J.-Q. Huang, M.-Q. Zhao, Q. Zhang, X.-B. Cheng, X.-Y. Liu, W.-Z. Qian, F. Wei, Nanoarchitectured Graphene/CNT@Porous Carbon with Extraordinary Electrical Conductivity and Interconnected Micro/Mesopores for Lithium-Sulfur Batteries, Adv. Funct. Mater. 24 (2014) 2772–2781.
[5] S.-H. Chung, P. Han, R. Singhal, V. Kalra, A. Manthiram, Electrochemically Stable Rechargeable Lithium-Sulfur Batteries with a Microporous Carbon Nanofiber Filter for Polysulfide, Adv. Energy Mater. 5 (2015) 1500738.
[6] J. Schuster, G. He, B. Mandlmeier, T. Yim, K.T. Lee, T. Bein, L.F. Nazar, Spherical Ordered Mesoporous Carbon Nanoparticles with High Porosity for Lithium-Sulfur Batteries, Angew. Chem. Int. Ed. 51 (2012) 3591–3595.
[7] X.-B. Cheng, J.-Q. Huang, Q. Zhang, H.-J. Peng, M.-Q. Zhao, F. Wei, Aligned carbon nanotube/sulfur composite cathodes with high sulfur content for lithium–sulfur batteries, Nano Energy 4 (2014) 65–72.
[8] Y. Fu, Y.-S. Su, A. Manthiram, Highly Reversible Lithium/Dissolved Polysulfide Batteries with Carbon Nanotube Electrodes, Angew. Chem. 125 (2013) 7068–7073.
[9] G. Zhou, L.-C. Yin, D.-W. Wang, L. Li, S. Pei, I.R. Gentle, F. Li, H.-M. Cheng, Fibrous Hybrid of Graphene and Sulfur Nanocrystals for High-Performance Lithium-Sulfur Batteries, ACS Nano 7 (2013) 5367–5375.
[10] X. Yang, L. Zhang, F. Zhang, Y. Huang, Y. Chen, Sulfur-Infiltrated Graphene-Based Layered Porous Carbon Cathodes for High-Performance Lithium-Sulfur Batteries, ACS Nano 8 (2014) 5208–5215.
[11] S.-H. Chung, A. Manthiram, A Polyethylene Glycol-Supported Microporous Carbon Coating as a Polysulfide Trap for Utilizing Pure Sulfur Cathodes in Lithium-Sulfur Batteries, Adv. Mater. 26 (2014) 7352–7357.
[12] Q. Pang, X. Liang, C.Y. Kwok, L.F. Nazar, Advances in lithium–sulfur batteries based on multifunctional cathodes and electrolytes, Nat. Energy 1 (2016) 16132.
[13] C. Zhang, J.J. Biendicho, T. Zhang, R. Du, J. Li, X. Yang, J. Arbiol, Y. Zhou, J.R. Morante, A. Cabot, Combined High Catalytic Activity and Efficient Polar Tubular Nanostructure in Urchin-Like Metallic NiCo2Se4 for High-Performance Lithium-Sulfur Batteries, Adv. Funct. Mater. 29 (2019) 1903842.
[14] L. Tan, X. Li, Z. Wang, H. Guo, J. Wang, Lightweight Reduced Graphene Oxide@MoS2 Interlayer as Polysulfide Barrier for High-Performance Lithium-Sulfur Batteries, ACS Appl. Mater. Interfaces 10 (2018) 3707–3713.
[15] P. Zeng, M. Chen, S. Jiang, Y. Li, X. Xie, H. Liu, X. Hu, C. Wu, H. Shu, X. Wang, Architecture and Performance of the Novel Sulfur Host Material Based on Ti2O3 Microspheres for Lithium-Sulfur Batteries, ACS Appl. Mater. Interfaces 11 (2019) 22439–22448.
[16] J. He, Y. Chen, A. Manthiram, MOF-derived Cobalt Sulfide Grown on 3D Graphene Foam as an Efficient Sulfur Host for Long-Life Lithium-Sulfur Batteries, iScience (2018) 36–43.
[17] G. Ai, Q. Hu, L. Zhang, K. Dai, J. Wang, Z. Xu, Y. Huang, B. Zhang, D. Li, T. Zhang, G. Liu, W. Mao, Investigation of the Nanocrystal CoS2 Embedded in 3D Honeycomb-like Graphitic Carbon with a Synergistic Effect for High-Performance Lithium Sulfur Batteries, ACS Appl. Mater. Interfaces 11 (2019) 33987–33999.
[18] M. Li, Y. Zhang, Z. Bai, W.W. Liu, T. Liu, J. Gim, G. Jiang, Y. Yuan, D. Luo, K. Feng, R.S. Yassar, X. Wang, Z. Chen, J. Lu, A Lithium-Sulfur Battery using a 2D Current Collector Architecture with a Large-Sized Sulfur Host Operated under High Areal Loading and Low E/S Ratio, Adv. Mater. 30 (2018) 1804271.
[19] G. Chen, W. Zhong, Y. Li, Q. Deng, X. Ou, Q. Pan, X. Wang, X. Xiong, C. Yang, M. Liu, Rational Design of TiO–TiO2 Heterostructure/Polypyrrole as a Multifunctional Sulfur Host for Advanced Lithium-Sulfur Batteries, ACS Appl. Mater. Interfaces 11 (2019) 5055–5063.
[20] A. Bhargav, M.E. Bell, J. Karty, Y. Cui, Y. Fu, A Class of Organopolysulfides As Liquid Cathode Materials for High-Energy-Density Lithium Batteries, ACS Appl. Mater. Interfaces 10 (2018) 21084–21090.
[21] H.-J. Peng, J.-Q. Huang, X.-B. Cheng, Q. Zhang, Review on High-Loading and High-Energy Lithium-Sulfur Batteries, Adv. Energy Mater. 7 (2017) 1700260.
[22] T. Xu, J. Song, M.L. Gordin, H. Sohn, Z. Yu, S. Chen, D. Wang, Mesoporous Carbon-Carbon Nanotube–Sulfur Composite Microspheres for High-Areal-Capacity Lithium-

Sulfur Battery Cathodes, ACS Appl. Mater. Interfaces 5 (2013) 11355–11362.
[23] Q. Pang, X. Liang, C.Y. Kwok, J. Kulisch, L.F. Nazar, A Comprehensive Approach toward Stable Lithium-Sulfur Batteries with High Volumetric Energy Density, Adv. Energy Mater. 7 (2017) 1601630.
[24] H.-J. Peng, W.-T. Xu, L. Zhu, D.-W. Wang, J.-Q. Huang, X.-B. Cheng, Z. Yuan, F. Wei, Q. Zhang, 3D Carbonaceous Current Collectors: The Origin of Enhanced Cycling Stability for High-Sulfur-Loading Lithium-Sulfur Batteries, Adv. Funct. Mater. 26 (2016) 6351–6358.
[25] Z. Cheng, Z. Xiao, H. Pan, S. Wang, R. Wang, Elastic Sandwich-Type rGO–VS2/S Composites with High Tap Density: Structural and Chemical Cooperativity Enabling Lithium-Sulfur Batteries with High Energy Density, Adv. Energy Mater. 8 (2018) 1702337.
[26] C. Zhang, W. Lv, Y. Tao, Q.-H. Yang, Towards superior volumetric performance: design and preparation of novel carbon materials for energy storage, Energy Environ. Sci. 8 (2015) 1390–1403.
[27] M. Li, Y. Zhang, F. Hassan, W. Ahn, X. Wang, W.W. Liu, G. Jiang, Z. Chen, Compact high volumetric and areal capacity lithium sulfur batteries through rock salt induced nano-architectured sulfur hosts, J. Mater. Chem. A 5 (2017) 21435–21441.
[28] Y. Zhao, W. Zhu, G.Z. Chen, E.J. Cairns, Polypyrrole/TiO2 nanotube arrays with coaxial heterogeneous structure as sulfur hosts for lithium sulfur batteries, J. Power Sources 327 (2016) 447–456.
[29] Z.-Z. Yang, H.-Y. Wang, L. Lu, C. Wang, X.-B. Zhong, J.-G. Wang, Q.-C. Jiang, Hierarchical TiO2 spheres as highly efficient polysulfide host for lithium-sulfur batteries, Scientific Reports 6 (2016) 22990.
[30] B. Ding, L. Shen, G. Xu, P. Nie, X. Zhang, Encapsulating sulfur into mesoporous TiO2 host as a high performance cathode for lithium–sulfur battery, Electrochim. Acta 107 (2013) 78–84.
[31] X.Z. Ma, B. Jin, H.Y. Wang, J.Z. Hou, X.B. Zhong, H.H. Wang, P.M. Xin, S-TiO2 composite cathode materials for lithium/sulfur batteries, J. Electroanal. Chem. 736 (2015) 127–131.
[32] G. Liang, J. Wu, X. Qin, M. Liu, Q. Li, Y.-B. He, J.-K. Kim, B. Li, F. Kang, Ultrafine TiO2 Decorated Carbon Nanofibers as Multifunctional Interlayer for High-Performance Lithium-Sulfur Battery, ACS Appl. Mater. Interfaces 8 (2016) 23105–23113.
[33] R. Dharmasena, A.K. Thapa, R.K. Hona, J. Jasinski, M.K. Sunkara, G.U. Sumanasekera, Mesoporous TiO2 coating on carbon–sulfur cathode for high capacity Li–sulfur battery, RSC Adv. 8 (2018) 11622–11632.
[34] D. Morphew, D. Chakrabarti, Clusters of anisotropic colloidal particles: From colloidal molecules to supracolloidal structures, Current Opin. Colloid Interf. Sci. 30 (2017) 70–80.
[35] C.X. Du, G. van Anders, R.S. Newman, S.C. Glotzer, Shape-driven solid–solid transitions in colloids, Proc. Natl. Acad. Sci. 114 (2017) E3892–E3899.
[36] Z. Li, Z. Xiao, S. Wang, Z. Cheng, P. Li, R. Wang, Engineered Interfusion of Hollow Nitrogen-Doped Carbon Nanospheres for Improving Electrochemical Behavior and Energy Density of Lithium-Sulfur Batteries, Adv. Funct. Mater. 29 (2019) 1902322.
[37] J. Li, B. Ding, G. Xu, L. Hou, X. Zhang, C. Yuan, Enhanced cycling performance and electrochemical reversibility of a novel sulfur-impregnated mesoporous hollow TiO2 sphere cathode for advanced Li–S batteries, Nanoscale 5 (2013) 5743–5746.
[38] X. Liu, J.-Q. Huang, Q. Zhang, L. Mai, Nanostructured Metal Oxides and Sulfides for Lithium-Sulfur Batteries, Adv. Mater. 29 (2017) 1601759.
[39] Z. Wei Seh, W. Li, J.J. Cha, G. Zheng, Y. Yang, M.T. McDowell, P.-C. Hsu, Y. Cui, Sulphur–TiO2 yolk–shell nanoarchitecture with internal void space for long-cycle lithium–sulphur batteries. Nat. Commun., 4 (2013) 1331.
[40] X. Wang, T. Gao, X. Fan, F. Han, Y. Wu, Z. Zhang, J. Li, C. Wang, Tailoring Surface Acidity of Metal Oxide for Better Polysulfide Entrapment in Li-S Batteries, Adv. Funct. Mater. 26 (2016) 7164–7169.
[41] Q. Pang, D. Kundu, M. Cuisinier, L.F. Nazar, Surface-enhanced redox chemistry of polysulphides on a metallic and polar host for lithium-sulphur batteries, Nat. Commun. 5 (2014) 4759.
[42] X. Liang, C. Hart, Q. Pang, A. Garsuch, T. Weiss, L.F. Nazar, A highly efficient polysulfide mediator for lithium–sulfur batteries, Nat. Commun. 6 (2015) 5682.
[43] T. Lei, Y. Xie, X. Wang, S. Miao, J. Xiong, C. Yan, TiO2 Feather Duster as Effective Polysulfides Restrictor for Enhanced Electrochemical Kinetics in Lithium-Sulfur Batteries, Small 13 (2017) 1701013.
[44] L. Li, L. Chen, S. Mukherjee, J. Gao, H. Sun, Z. Liu, X. Ma, T. Gupta, C.V. Singh, W. Ren, H.-M. Cheng, N. Koratkar, Phosphorene as a Polysulfide Immobilizer and Catalyst in High-Performance Lithium-Sulfur Batteries, Adv. Mater. 29 (2017) 1602734.
[45] Y. Li, Q. Cai, L. Wang, Q. Li, X. Peng, B. Gao, K. Huo, P.K. Chu, Mesoporous TiO2 Nanocrystals/Graphene as an Efficient Sulfur Host Material for High-Performance Lithium-Sulfur Batteries, ACS Appl. Mater. Interfaces 8 (2016) 23784–23792.
[46] J.-Q. Huang, Z. Wang, Z.-L. Xu, W.G. Chong, X. Qin, X. Wang, J.-K. Kim, Three-Dimensional Porous Graphene Aerogel Cathode with High Sulfur Loading and Embedded TiO2 Nanoparticles for Advanced Lithium-Sulfur Batteries, ACS Appl. Mater. Interfaces 8 (2016) 28663–28670.
[47] Y. Zhang, S. Yao, R. Zhuang, K. Luan, X. Qian, J. Xiang, X. Shen, T. Li, K. Xiao, S. Qin, Shape-controlled synthesis of Ti4O7 nanostructures under solvothermal-assisted heat treatment and its application in lithium-sulfur batteries, J. Alloys Compd. 729 (2017) 1136–1144.
[48] T. An, D. Deng, M. Lei, Q.-H. Wu, Z. Tian, M. Zheng, Q. Dong, MnO modified carbon nanotubes as a sulfur host with enhanced performance in Li/S batteries, J. Mater. Chem. A 4 (2016) 12858–12864.
[49] D. Gueon, J.T. Hwang, S.B. Yang, E. Cho, K. Sohn, D.-K. Yang, J.H. Moon, Spherical Macroporous Carbon Nanotube Particles with Ultrahigh Sulfur Loading for Lithium-Sulfur Battery Cathodes, ACS Nano 12 (2018) 226–233.
[50] M. Yu, J. Ma, H. Song, A. Wang, F. Tian, Y. Wang, H. Qiu, R. Wang, Atomic layer deposited TiO2 on a nitrogen-doped graphene/sulfur electrode for high performance lithium–sulfur batteries, Energy Environ. Sci. 9 (2016) 1495–1503.
[51] X. Qin, J. Wu, Z.-L. Xu, W.G. Chong, J.-Q. Huang, G. Liang, B. Li, F. Kang, J.-K. Kim, Electrosprayed multiscale porous carbon microspheres as sulfur hosts for long-life lithium-sulfur batteries, Carbon 141 (2019) 16–24.
[52] S.-H. Chung, A. Manthiram, Designing Lithium-Sulfur Batteries with High-Loading Cathodes at a Lean Electrolyte Condition, ACS Appl. Mater. Interfaces 10 (2018) 43749–43759.
[53] K. Sun, A.K. Matarasso, R.M. Epler, X. Tong, D. Su, A.C. Marschilok, K.J. Takeuchi, E.S. Takeuchi, H. Gan, Effect of Electrolyte on High Sulfur Loading Li-S Batteries, J. Electrochem. Soc. 165 (2018) A416–A423.
[54] N.B. Emerce, D. Eroglu, Effect of Electrolyte-to-Sulfur Ratio in the Cell on the Li-S Battery Performance, J. Electrochem. Soc. 166 (2019) A1490–A1500.
[55] H. Kwack, J. Lee, W. Jo, Y.-J. Kim, H. Noh, H. Chu, H.-T. Kim, Rational Design of Highly Packed, Crack-Free Sulfur Electrodes by Scaffold-Supported Drying for Ultrahigh-Sulfur-Loaded Lithium-Sulfur Batteries, ACS Appl. Mater. Interfaces 11 (2019) 29849–29857.
[56] Z. Cheng, H. Pan, J. Chen, X. Meng, R. Wang, Separator Modified by Cobalt-Embedded Carbon Nanosheets Enabling Chemisorption and Catalytic Effects of Polysulfides for High-Energy-Density Lithium-Sulfur Batteries, Adv. Energy Mater. 9 (2019) 1901609.